16

Automatic Space Rendezvous and Docking Using Second Order Sliding Mode Control

Christian Tournes[1], Yuri Shtessel[2] and David Foreman[3]
[2]*University of Alabama Huntsville*
[1,3]*Davidson Technologies Inc*
USA

1. Introduction

This chapter presents a Higher Order Sliding Mode (HOSM) Control for automatic docking between two space vehicles. The problem considered requires controlling the vehicles' relative position and relative attitude. This type of problem is generally addressed using optimal control techniques that are, unfortunately, not robust. The combination of optimum control and Higher Order Sliding Mode Control provides quasi-optimal robust solutions. Control of attitude includes a receiver vehicle passive mode option where the pursuing vehicle controls the relative attitude using the active pixels of a camera viewing a network of lights placed on the receiving vehicle, which by sharing considerable commonality with manual operations allows possible human involvement in the docking process.

2. Problem description

The complexity of satellite formation and automatic space docking arises from the formulation of Wilshire equations. These equations are nonlinear and exhibit coupling of normal and longitudinal motions. The problem is compounded by the characteristics of the on/off thrusters used. Typical solutions to the problem involve application of optimal control. The problem with optimal control is that it is not robust and it only works well when a perfectly accurate dynamical model is used. This subject has been investigated extensively by the research community (Wang, 1999), (Tournes, 2007). Since this is a navigation and control problem involving two bodies, one question is how to obtain the measurements to be used. Of course a data link from the receiving vehicle to inform the pursuer about its state can be used, whereby the pursuer receives the current position velocity and attitude state of the receiving vehicle. One could also mount distance measurement equipment on the vehicles such as a Lidar to provide accurate range and range rate measurements. The exchange of attitude represents a larger challenge, as the relative motion will be the difference of the measurements/estimations by separate Inertial Measurement Units (IMU) of their attitude. Such a difference will contain the drift and the noise of two IMUs.
The transversal aspect of this chapter presents lateral and longitudinal guidance algorithms, based on measurements of range and range rate without regard to the source of these

measurements which could be provided by a Lidar system (Tournes, 2007) or interpreted from visible cues using a pattern of reference lights.

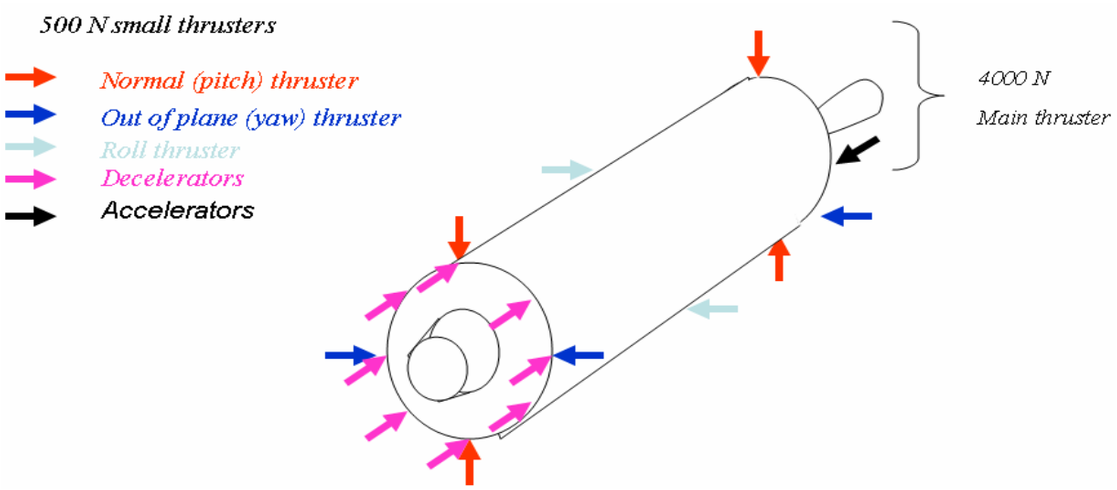

Fig. 1. Notional vehicle.

The attitude aspect presents a workable solution that does not require any reporting by the receiving unit and is based on a pattern of reference lights, that when viewed by the pursuer would allow the latter to evaluate the relative attitude orientation error. The quaternion representing the relative attitude is estimated in real time by a nonlinear curvefit algorithm and is used as the feedback of a second order sliding mode attitude control algorithm.
For simulation purposes, we assumed the pursuing vehicle (as shown in Fig. 1) to be similar in characteristics to ESA's Automated Transfer Vehicle (ESA 2006). Its initial mass is 10000 kg. It is equipped with a main / sustainer orientable thruster providing 4000 N thrust. Twenty small thrusters of 500 N are used by pairs to steer roll, pitch, and yaw attitude as well as lateral and normal motion. Regarding axial dynamics, we assume that several axial thrusters could be used to achieve axial deceleration. We assume that using all of them would provide a "maximum" braking; using half would provide a "medium" breaking; and using a quarter would provide "small" braking. A major goal in the study was to obtain extremely small velocity, position and attitude errors at the docking interface.

3. Governing equations and problem formulation

Equations governing the relative motion of the pursuer with respect to the pursued vehicle are along in-track, out of plane and normal axis represented by Wilshire equations (Chobotov, 2002).

$$\begin{aligned}
\mathbf{r}_{sv} &= \mathbf{r}_T + \boldsymbol{\rho} \\
\ddot{\mathbf{r}}_{sv} &= \ddot{\mathbf{r}}_T + \ddot{\boldsymbol{\rho}} + 2(\boldsymbol{\omega} \times \dot{\boldsymbol{\rho}}) + \dot{\boldsymbol{\omega}} \times \boldsymbol{\rho} + \boldsymbol{\omega} \times (\boldsymbol{\omega} \times \boldsymbol{\rho}) \\
\ddot{\mathbf{r}}_{sv} &= \mathbf{g} + \frac{\mathbf{F}}{m} = \mathbf{g} + \boldsymbol{\Gamma} \\
\ddot{\boldsymbol{\rho}} &= \boldsymbol{\Gamma} + \mathbf{f(t)}
\end{aligned} \tag{1}$$

Where $\mathbf{r}_{sv}, \mathbf{r}_T, \boldsymbol{\rho}$ represent respectively the space vehicle position pursued vehicle position and relative position vectors; Γ, g are the thrust and gravity accelerations.

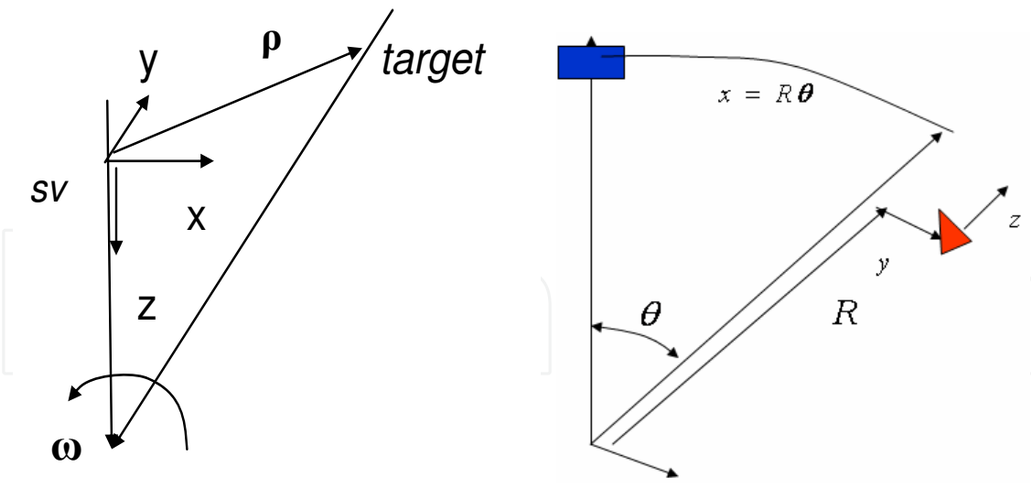

Fig. 2. System of axes used.

3.1 Translational dynamics

The system of axes used is shown in Fig. 2. Equation (1) is linearized, assuming that the thrust **F** is aligned with the pursuer longitudinal axis. Expressing the three components of gravity vector **g** as function of the pursuer position vector, one obtains

$$\begin{aligned}
&\ddot{x} = f_x(.) + \frac{F_x}{m}; \quad f_x(.) = -\mu\frac{x}{r^3} + 2\omega\dot{z} + \dot{\omega}z + \omega^2 x \\
&\ddot{y} = f_y(.) + \frac{F_y}{m}; \quad f_y(.) = -\mu\frac{y}{r^3} \\
&\ddot{z} = f_z(.) + \frac{F_z}{m}; \quad f_z(.) = -\mu\frac{z + r_T}{r^3} + \frac{\mu}{r_T^2} - 2\omega\dot{x} - \dot{\omega}x + \omega^2 z
\end{aligned} \tag{2}$$

Where x, y, z are relative coordinates; ω is a rotational speed of a frame connected to the pursued vehicle, μ represents the gravitational constant. Functions: $f_x(.)$, $f_y(.)$, $f_z(.)$ represent the effects in Eq. (1) other than caused by thrust and are treated as disturbances. They are smooth functions which tend to zero as the vehicles get closer. When variable attitude mode is in effect, Eq. (2) is generalized to a form

$$\ddot{x} = \Gamma\sqrt{1-\delta_y^2}\sqrt{1-\delta_z^2}\,\delta_x + f_x(.); \ddot{y} = \Gamma\sqrt{1-\delta_z^2}\,\delta_y + f_y(.); \ddot{z} = \Gamma\delta_z + f_z(.) \tag{3}$$

Here, $\Gamma = F/m$; F (the magnitude of the thrust) can take three discrete values, the vehicle mass m varies slowly with time, δ_x can take discrete values 1,-0, 1. Pursuer pitch and yaw attitude angles are defined as $\theta = asin(\delta_z)$ and $\psi = atan2(\delta_x\sqrt{1-\delta_y^2}, \delta_y)$ respectively.
When fixed attitude mode is in effect, Eq. (2) is written as:

$$\ddot{z} = f_z(.) + \frac{F}{m}u_z; \quad u_z = \{-1,0,1\}; \ddot{y} = f_y(.) + \frac{F}{m}u_y; \quad u_y = \{-1,0,1\}; \ddot{x} = f_x(.) + \frac{F}{m}u_x; \quad u_x = \{-1,0,1\} \tag{4}$$

3.2 Attitude dynamics

The body attitude is represented by quaternion $\mathbf{Q}_{(.)}^{body}$ the dynamics of which is governed by

$$\dot{\mathbf{Q}}_{(.)}^{body} = -\frac{1}{2}\begin{bmatrix} 0 & p & q & rr \\ -p & 0 & -rr & q \\ -q & rr & 0 & -p \\ -rr & -q & p & 0 \end{bmatrix}\mathbf{Q}_{(.)}^{body} \tag{5}$$

Where (.) represents some non rotating reference, i.e. Earth Centered Inertial and Where *p, q, rr* represent the body rates expressed in the body frame. An alternate notation, using quaternion multiplication (Kuipers, 1999) is:

$$\dot{\mathbf{Q}}_{(.)}^{body} = \mathbf{Q}_{(.)}^{body}\,\boldsymbol{\Omega}$$

The dynamics *p, q, rr* are governed by

$$\dot{\boldsymbol{\Omega}} = \begin{bmatrix} \dot{p} \\ \dot{q} \\ \dot{r}r \end{bmatrix} = -\mathbf{I}^{-1}\boldsymbol{\Omega}\times\mathbf{I} + \mathbf{I}^{-1}\begin{bmatrix} \frac{l}{2}r_p F_p \delta_p \\ (x_{\delta q} - x_{cg})F_q\delta_q \\ -(x_{\delta q} - x_{cg})F_q\delta_{rr} \end{bmatrix} \tag{6}$$

Where $\mathbf{I}$ represent the vehicle matrix of inertia, $\boldsymbol{\Omega}$ the rotation matrix in body axes and $F_p, F_q, r_p, x_q, x_{cg}, \delta_p, \delta_q, \delta_{rr}$ represent respectively roll, pitch/yaw thruster maximum force, roll thrusters radial position, pitch/yaw thruster axial position, and corresponding normalized control amplitudes in roll, pitch and yaw.

3.3 Problem formulation

3.3.1 Lateral control: The control must steer the vehicle position to the prescribed orbital plane and orbit altitude. For that matter during the *initial rendezvous*, out-of-plane and relative orbit positions with respect to pursued vehicle are calculated at the onset of the maneuver. The HOSM lateral trajectory control calculates required acceleration to follow the desired approach profile and calculates the required body attitude represented by quaternion $\mathbf{Q}^{*body}_{(.)}$. During subsequent drift, braking and final docking phases the pursuer is maintained in the orbital plane and at the correct altitude by means of on-off HOSM control applied by the corresponding thrusters.

3.3.2 Longitudinal control: During initial *rendezvous* the pursuer accelerates using the main thrust/sustainer. Corresponding thrust is shut down when the pursuer is in the orbital plane, has attained the pursued vehicle's orbit altitude and desired closing rate. During the drift segment no longitudinal control is applied. The braking segment begins at a range function of the range rate. Following coast, braking is applied until reaching the terminal sliding mode condition. On-off deceleration pulses are then commanded by the HOSM longitudinal control.

3.3.3 Attitude control: During the initial rendezvous, continuous HOSM controls the attitude such that $\mathbf{Q}_{(.)}^{body} \rightarrow \mathbf{Q}^{*body}_{(.)}$ where $\mathbf{Q}_{(.)}^{body}$ represents current body attitude. During following segments the pursuing vehicle regulates its body attitude so that $\mathbf{Q}_{(.)}^{body} \rightarrow \mathbf{Q}\#_{(.)}^{body}$ where $\mathbf{Q}\#_{(.)}^{body}$ represents the attitude of the pursued vehicle.

4. Why higher order sliding mode control

HOSM control is an emerging (less than 10 years old) control technique (Shtessel, 2003), (Shkolnikov, 2000), (Shtessel, 2000), (Shkolnikov, 2005), (Tournes, 2006), (Shtessel, 2010) which represents a game changer. It should not be confused with first order sliding mode control which has been used for the last 30 years. Its power resides in four mathematically demonstrated properties:

1. **Insensitivity to matched disturbances:** Consider a system of relative degree n, with its output tracking error dynamics represented as:

$$x^{(n)} = f(x,t) - u \tag{7}$$

where $f(x,t)$ represents some unknown disturbance. A convergence function $u = C(x, \dot{x}, ..x^{(n-1)})$ is selected so that the output tracking error x in Eq. (7) and its consecutive derivatives up to degree $n-1$ converge to zero in finite time in the presence of the disturbance $f(x,t)$ provided that $|f(x,t)| < M$ is bounded. In this application, such a bound exists (Chobotov, 2002), (Wang, 1999). This property of HOSM control is inherited from classical sliding mode control (SMC). Being implemented in discrete time, the output tracking error is not driven to precisely zero but is ultimate bounded in the sliding mode with sliding accuracy proportional to the k^{ith} power of time increment Δt. This property makes HOSM an enhanced-accuracy robust control technique applicable to controllers and to observer design.
2. **Dynamical collapse:** Unlike traditional control techniques that seek asymptotic convergence, HOSM achieves finite time convergence in systems with arbitrary relative degree, just as classical SMC achieves the same result for the system with relative degree one. This is much more than an academic distinction; it means that when the sliding mode is reached the effective transfer function of inner loops with relative degree greater than one becomes an identity.
3. **Continuous / smooth guidance laws:** HOSM controllers can yield continuous and even smooth controls that are applicable in multiple-loop integrated guidance/autopilot control laws.
4. **Continuous / Discontinuous actuators:** HOSM techniques are nonlinear robust control techniques. When discontinuous actuators such as on-off thrusters must be used, all linear control laws require a re-design into a discontinuous control law that approximates the effects of the initial control law. HOSM design produces directly, when need arises, a discrete pulse width modulated control law that achieves the same level of accuracy as a linear control law.

5. Docking strategy

It is assumed in Fig. 3 that the automatic docking starts at a relatively large distance (>40-50 km). The pursuer, during *Initial Rendezvous* manages using its main thrust / sustainer to get in a coplanar circular orbit with altitude equal to that of the receiving vehicle, but with a slightly higher longitudinal velocity. Maintaining this altitude will require infrequent thruster firings by the pursuer. Alternately, one could place the pursuer on a circular coplanar orbit consistent with its longitudinal velocity and design the control law to track the orbit associated to its current velocity which "in time" will end up being the same as the

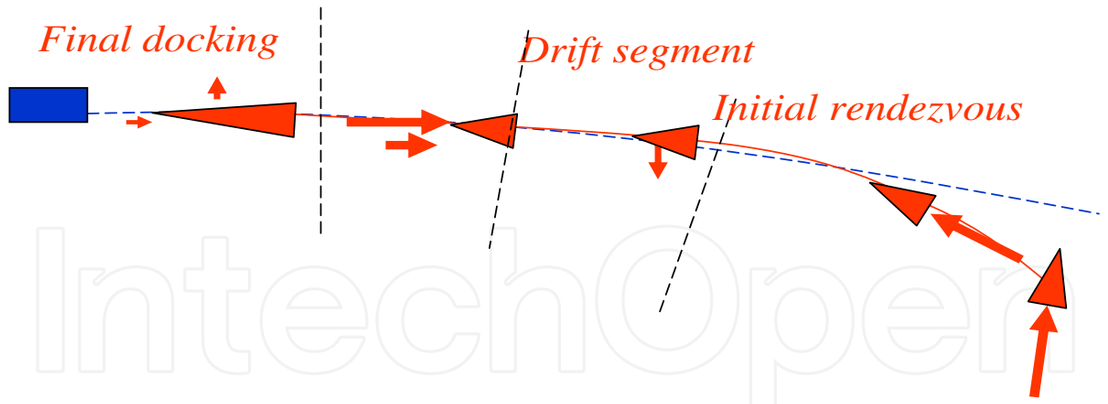

Fig. 3. Docking strategy.

pursued vehicle altitude. During the initial rendezvous, the pursuing vehicle is set to the desired drift velocity relative to the pursued vehicle. This maneuver is represented by trajectory 0-1-2 in the phase portrait of Fig. 4. During this initial segment, a varying attitude mode is applied. The transition from variable attitude to fixed attitude takes place when the normal and out-of plane errors become lower than a prescribed threshold defined as

$$V1 = (y^2 + z^2 + \dot{y}^2 + \dot{z}^2); \quad V1 < \varepsilon 3 \tag{9}$$

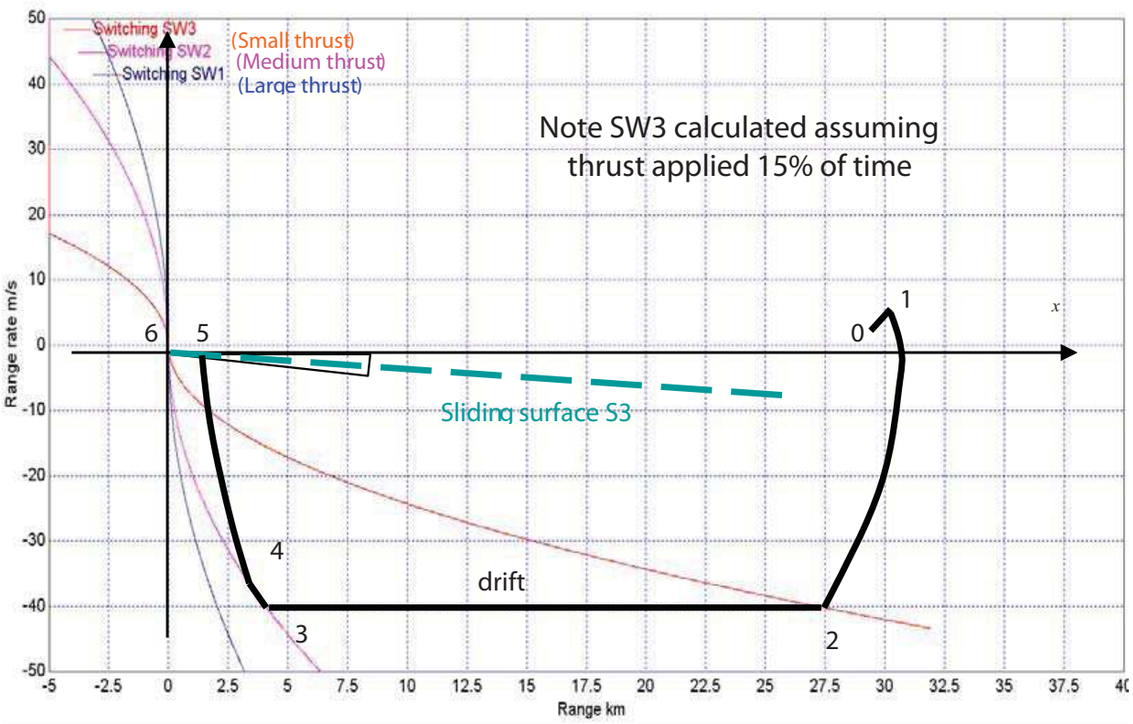

Fig. 4. Longitudinal control strategy.

During the drift segment, normal and lateral control is applied to keep the pursuer vehicle at the prescribed altitude and in the prescribed plane. The drift motion (2-3) begins with

$$V = (x^2 + y^2 + z^2 + \dot{x}^2 + \dot{y}^2 + \dot{z}^2); \quad V < \varepsilon \tag{10}$$

The end of the drift segment is calculated using Pontyagyn's Principle of Maximum. Three switching surfaces are defined as:

$$SW1 = x + \frac{sign(\dot{x})\dot{x}^2 m(t)}{2F_1}; SW2 = x + \frac{sign(\dot{x})\dot{x}^2 m(t)}{2F_2}; SW3 = x + \frac{sign(\dot{x})\dot{x}^2 m(t)}{2\alpha F_3} \tag{11}$$

Large, medium, or small thrust is applied as thresholds $SW1, SW2, SW3$ are reached depending on the braking strategy used and this thrust is applied until the distance from the terminal switching surface becomes small enough. At that point, the terminal thrust is shut down. The termination of the decelerating maneuver is governed by

$$\sigma_x = 2x + \dot{x}; \quad |\sigma_x| > \varepsilon 2 \tag{12}$$

Once (12) is satisfied, terminal docking begins: radial and out-of-plane errors are almost null and the only disturbance left is radial with a magnitude $f_z(.) = -2\omega\dot{x}$ and this has already been greatly reduced by previous in-track braking.

6. HOSM design of the relative navigation

6.1 Normal / Lateral control during initial rendezvous

During the initial phase of the rendezvous, the pursuing vehicle is steered by the continuous orientation of its main thruster/sustainer. We select the relative normal / lateral positions as the sliding variables. Given that the ultimate objective of this initial rendezvous is to set the pursuing vehicle in an orbit coplanar to the pursued vehicle's orbit and at the same altitude, we define $z^*(t)_{(.)}; (.) = radial, out\ of\ plane$ to be a profile joining initial pursuer vehicle with its terminal objective, this profile is designed to be terminally tangent to pursued vehicle orbit. The *initial rendezvous* objective is thus, to steer the pursuer trajectory so that $z(t) \to z^*(t)_{(.)}$. Sliding variable is chosen as:

$$\sigma_{(.)} = z_{(.)}{}^* - z_{(.)} \tag{13}$$

Applying the relative degree procedure, we differentiate twice the sliding variable before the control appears, with Eqs. (4, 13) we obtain a dynamics of sliding variable of relative degree two.

$$\begin{aligned} &\ddot{\sigma}_{(.)} = d - bu_{(.)}; (.)z, y \\ &d_{(.)} = \ddot{z}_{(.)} - f_{(.)}(.); b_{(.)} = \frac{F_{(.)}}{m} \end{aligned} \tag{14}$$

Consider sliding variable dynamics given by a system with a relative degree two.

$$\ddot{\sigma} = h(\sigma, \dot{\sigma}, t) + k(t)u_\delta, \quad k(t) > 0 \tag{15}$$

In the considered case, the controls are continuous. Define auxiliary sliding surfaces $s_{(.)}$ as dynamical sliding manifolds

$$\begin{aligned} s_{(.)} &= \dot{\sigma}_{(.)} + \varpi \left|\sigma_{(.)}\right|^{1/2} sign(\sigma_{(.)}) \\ s_{(.)} &\to 0 \Rightarrow \sigma_{(.)}, \dot{\sigma}_{(.)} \to 0 \end{aligned} \tag{16}$$

As the sliding manifolds are relative degree 1 with respect to the system, the controller is now relative degree 1 with respect to the sliding manifold. The corresponding Super-Twist controllers are given by:

$$u_{(.)} = Limit[-0.5, 0.5](-\alpha sign(s_{(.)}) \left|s_{(.)}\right|^{1/2} - \beta \int_0^t sign(s_{(.)}) d\tau \tag{17}$$

Where the Limit [,] is imposed because the relative attitude with respect to the trajectory must be bounded such as to leave enough longitudinal control authority to steer the longitudinal relative motion.

6.2 Normal / Lateral control during fixed attitude mode

After reaching the prescribed altitude and the prescribed orbital plane, normal/lateral on-off thrusters are used to keep the pursuing vehicle at the proper altitude and in the orbital plane.

With $k_m < k(t) < k_M$ and $\left|h(\sigma, \dot{\sigma}, t)\right| \le L$; it is shown (Edwards, 1998), (Utkin, 1999), (Levant, 2001), (Shtessel, 2003), (Shkolnikov, 2000), (Shtessel, 2000) that a sliding variable σ given by (10) is stabilized at zero altogether with its derivative $\dot{\sigma}$ in finite time by means of the SOSM controller

$$u = -\bar{\rho} \cdot sign(\dot{\sigma} + \lambda \left|\sigma\right|^{0.5} sign(\sigma)), \quad \lambda > 0, \quad \bar{\rho} > 0 \tag{18}$$

where $\bar{\rho} > \left(0.5\lambda^2 + L\right) / k_M$. This controller is called a *second order sliding mode controller with prescribed convergence law.* It is worth noting that the high frequency switching SOSM controller (18) achieves the finite time stabilization of σ and $\dot{\sigma}$ at zero in the presence of a bounded disturbance $h(\sigma, \dot{\sigma}, t)$.

Controller (18) yields on-off control that can be applied directly to the on-off thrusters. Here we choose $\lambda = 8\ rad / \sec$, and $\bar{\rho} = 0.1\ m / s^2$ is imposed by the acceleration achieved by the on-off thrusters.

6.3 Simulation

The Six Degrees of Freedom simulation was ran in Earth Centered Inertial Coordinates over rotating spherical Earth[1]. Attitude motion was calculated using Quaternions representing the body attitude with respect to ECI frame[2]. The simulation was calculated in normalized units with unit of length being the equatorial radius, the unit of velocity the circular velocity at the surface level, and the time unit the ratio of previous quantities. The results are presented in SI units and the gains used in normalized units converted to SI units.

[1] The simulation could be easily extended to work over oblate Earth. However since the problem is a problem of relative motion, this easy extension was not considered

[2] The problem to solve is a problem of relative attitude, and for that matter any other reference could have been chosen such as North East Down.

Integration step used was 10^{-6} normalized time units that is about 0.000806 sec. The integrations were performed using Runge-Kutta 4 algorithm build in the Vissim simulation software.

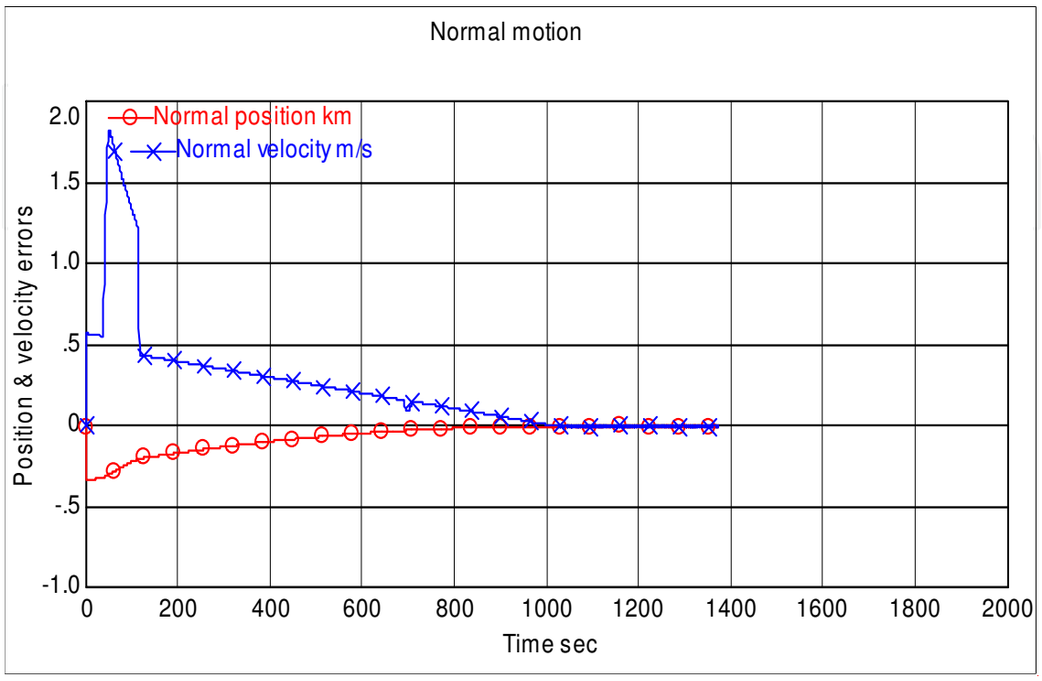

Fig. 5. Normal position and velocity error.

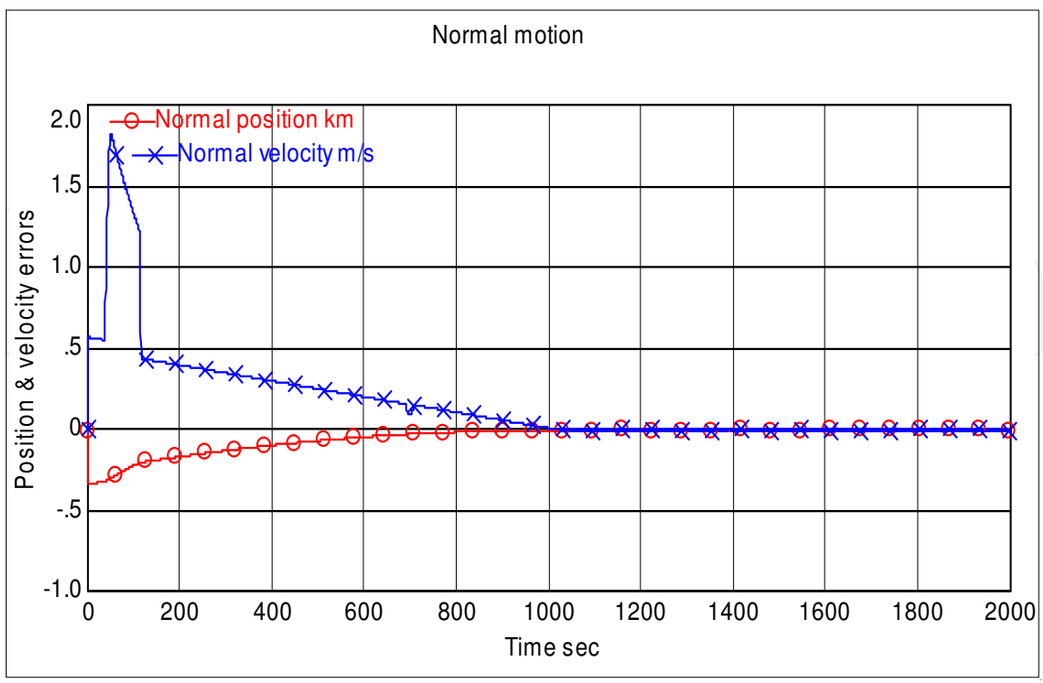

Fig. 6. Vehicle relative pitch attitude error.

The results Fig. 5 show that after the initial rendezvous normal/lateral distances to the receiving vehicle's orbit are kept within millimeters, millimeters /sec. Figure 6. depicts the corresponding vehicle attitude.

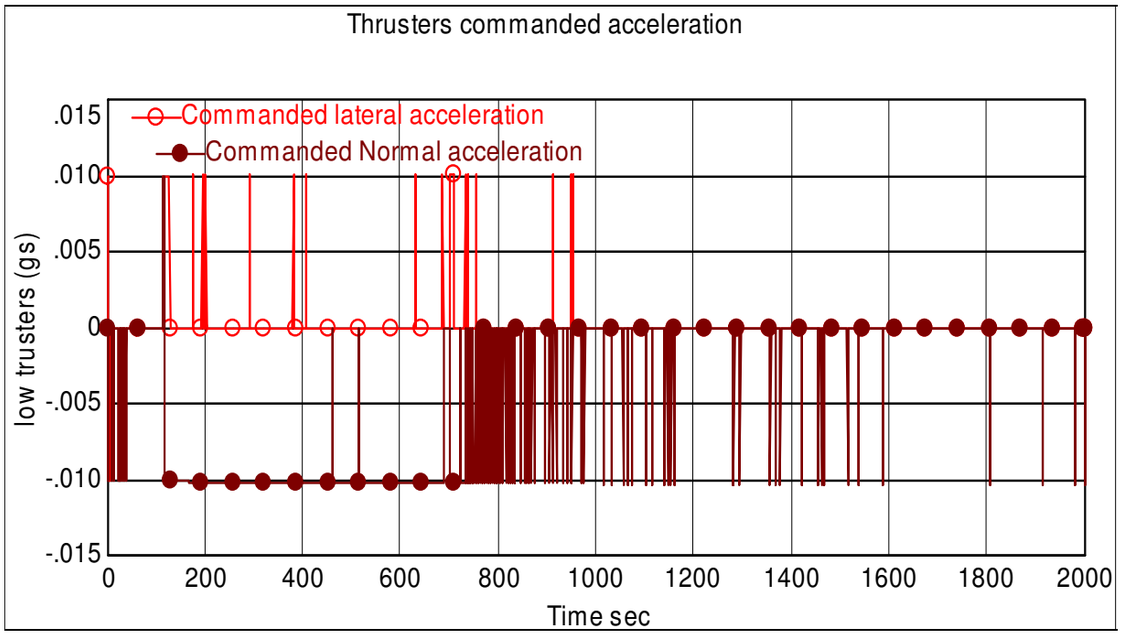

Fig. 7. Activity of the small thrusters.

The result Fig. 7 exhibits thruster commands during an important interval of activity in the segment 114-930 sec. The interval 114-537 corresponds to the drift segment during which the pursuing vehicle is at the same altitude that the pursued vehicle but has larger velocity by approximately 40 m/s. The interval 537-936 records deceleration to a much smaller longitudinal relative velocity. From there, as the longitudinal velocity is constantly reduced, the firing of normal thrusters becomes more and more infrequent. Conversely the activity of transversal thrusts reduces much more rapidly as this error is driven to zero.

6.3 Longitudinal control during terminal sliding mode phase

The prescribed longitudinal relative motion is defined by sliding variable
Figure 6. displays the corresponding vehicle normal and lateral (out-of-plane) thrusters' activity.

$$\sigma_x = \dot{x} + cx \tag{20}$$

When the longitudinal sliding surface is reached (when $\sigma_x \approx 0$), this forces the longitudinal velocity to reduce as the range becomes smaller. Using this surface the pulse width controller is given by

$$\begin{aligned} &w_x = -A sign(\sigma_x)|\sigma_x|^{1/2} - B\int_0^t sign(\sigma_x)d\tau;\ u_x = PWM(w_x) \\ &PWM(u) = DeadBand(1-\nu, u) + 0.5 + Triangle(1, \varepsilon) \\ &Triangle(A, f) = triangular\ wave\ amplitude = A,\ frequency = f \end{aligned} \tag{21}$$

6.4 Longitudinal breaking strategies and gates

Several control strategies have been analyzed which use braking maneuvers of different intensity and duration. We present hereafter the medium breaking strategy.

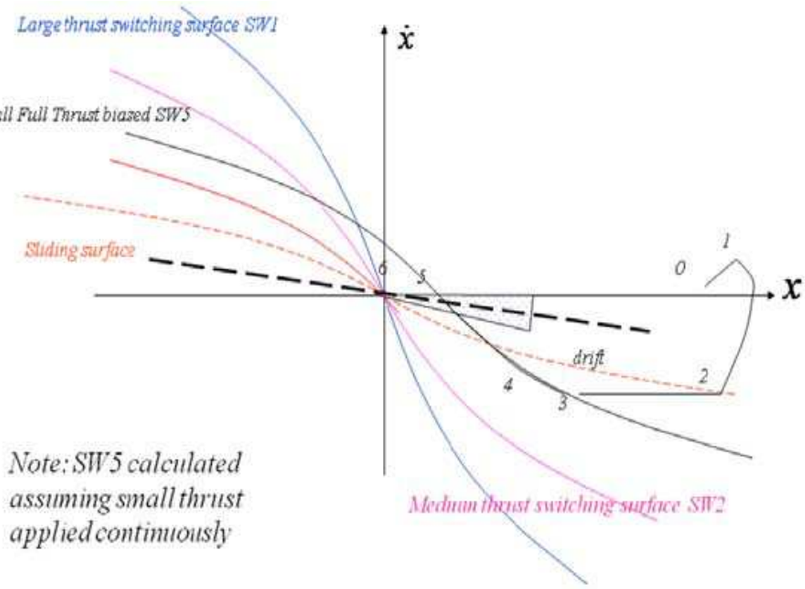

Fig. 8. Longitudinal control strategy 2 medium breaking.

Longitudinal control starts at point 1, the beginning of initial rendezvous. The pursuing vehicle accelerates using the main thruster / sustainer until point 2 when the relative prescribed closing velocity is reached. This point is selected such that a 15% duty cycle of small thruster deceleration would be required to steer the relative position and velocity approximately to zero. It is followed by a drift segment until reaching the second breaking curve at point 3, represented by a medium breaking stategy biased by some positive range.
The medium deceleration is applied from 3-5 until reaching the sliding surface. From 5-6 the longitudinal motion is governed by the linear manifold Eq. (12).
Results in Fig 9 show the variation of longitudinal range and range rate as functions of time. One can note that after significant initial variations in range and range rate, their values decrease asymptotically after reaching the sliding surface at t=914.

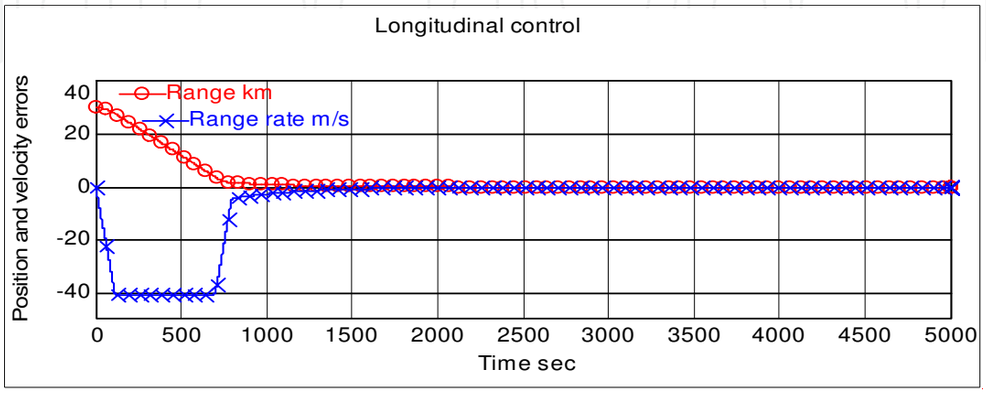

Fig. 9. Longitudinal control.

Results Fig. 10 show the absence of longitudinal control during the "drift" segment and also the continuous application of the "medium" deceleration from 700-796 sec. Results in Fig.10 show the pattern of longitudinal thrust. Starting on the left, one can note the sustainer thrust followed by the drift segment where no longitudinal thrust is applied, the deceleration pulse, then the deceleration segment where braking thrust is applied continuously;

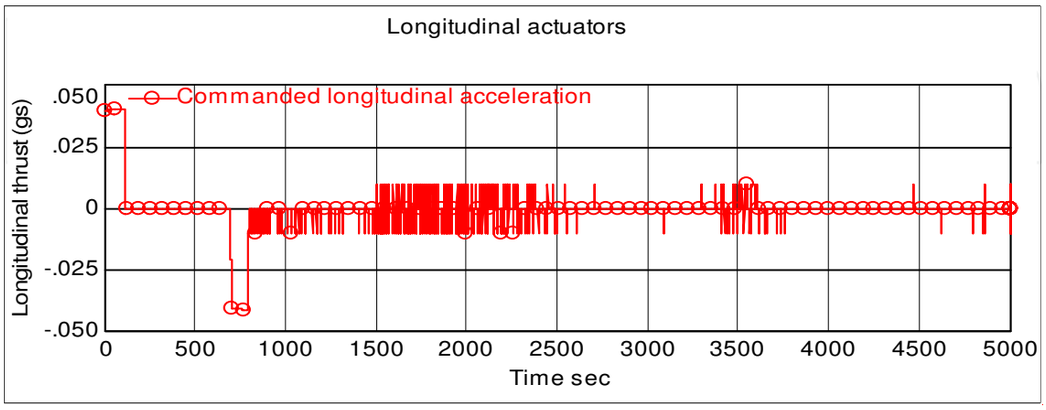

Fig. 10. Longitudinal thruster activity.

Results Fig. 10 also show the absence of longitudinal control during the "drift" segment and the continuous application of "medium" deceleration from 700-796 sec. Results in Fig. 10 show the pattern of longitudinal thrust. Starting on the left, one can note the sustainer thrust followed by the drift segment where no longitudinal thrust is applied, the deceleration pulse, then the deceleration segment where braking thrust is applied continuously; thereafter, the firing becomes sparser and the durations of the thrust pulses smaller, and reaches "soft kiss" conditions with range and range rate in the sub-millimeter and millimeter / sec. It is possible to make the docking faster by modifying parameter c in Eq. (20) and to interrupt it sooner as docking tolerances are reached. Another factor that may be considered in the automatic docking is the incorporation of cold gas thrusters to provide small and clean propulsive increments for final docking.

Three gateways are designed to check that the automatic docking is on track; equivalently, that provided the interceptor position is within the gate, docking can be pursued safely; specifically, that the margin of error they define can be corrected safely with available control authority.

For that matter we are going to present the gates from final to initial.

The third gateway is defined at the beginning of the deceleration The outer range is the minimum range such that if small thrusters are applied continously, the deceleration will achieve a zero velocity and distance from the receiving station. The deceleration must begin at the latest when intersecting the outside elliptical contour. The inner contour represents the minimum time for driving the longitudinal sliding variable to zero. The terminal deceleration in sliding mode must be initiated before reaching the inner contour.

At point 3 of Fig. 11, the pursuing vehicle begins medium braking, segment 3-5. Point 4 is at the intersection with the contour where there is enough stopping power to overcome the disturbances and stop at the origin using the small break. The breaking maneuver with small break must begin at the latest at point 4. The point 5 is designed to be on the intersection of the sliding manifold Eq. (12), with the small braking biased contour.

Evidently, the point 5 must be outside the inner elliptical contour that defines the minimum time needed to drive the terminal sliding surface to the origin.

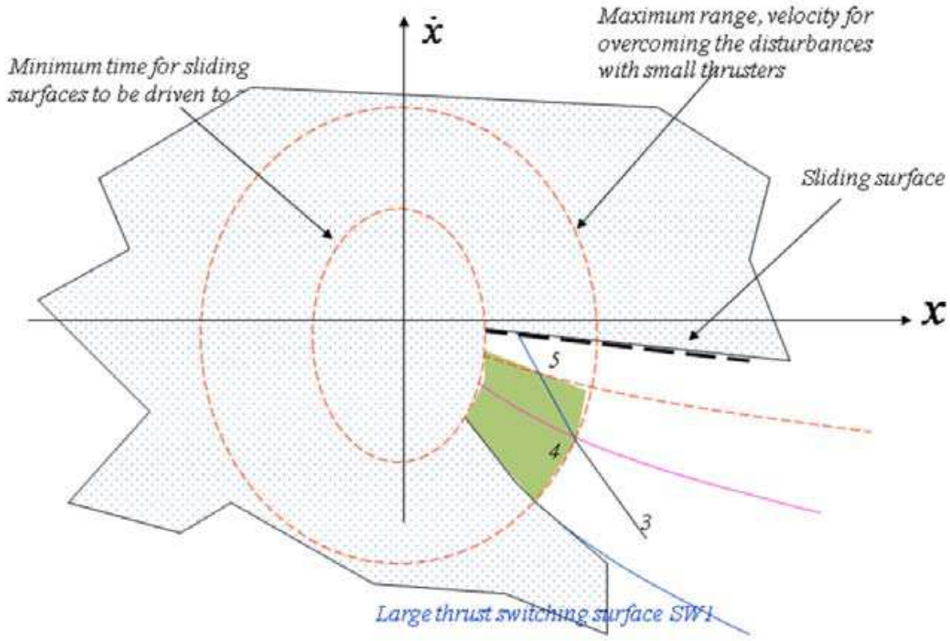

Fig. 11. Third gate.

The second gate Fig. 12 defines the drift segment. It begins at point 2; the intersection of the drift segment with SW3 and it ends at point 3 the beginning of the braking maneuver on biased SW5.

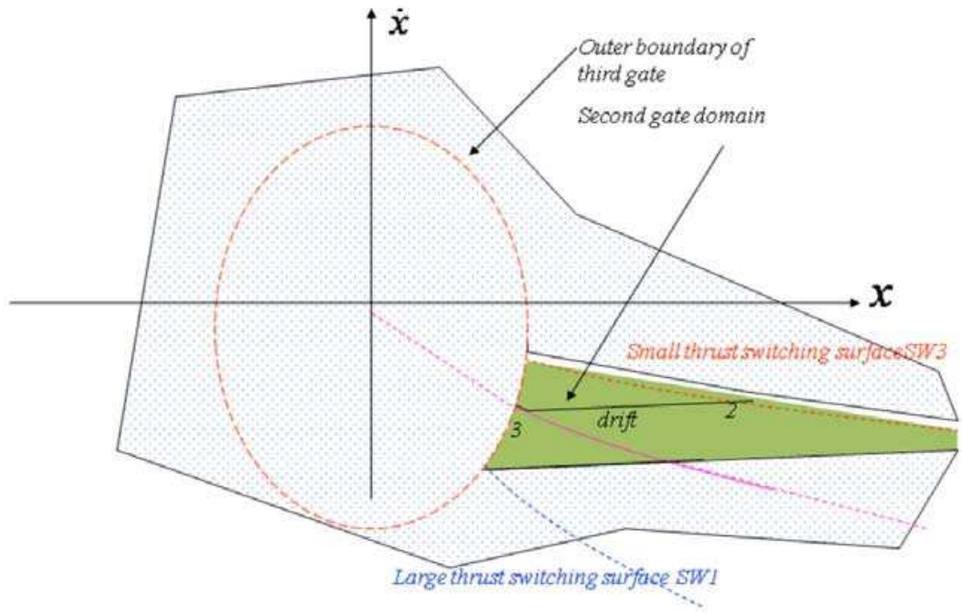

Fig. 12. Second gate.

The first gate (Fig. 13) defines the initial contour where the interceptor must be in the phase plane to intersect the small partial thrust SW3 with a viable drift velocity value and suffcient drift time. In any case the initial point 1 must be above SW3 and there is some latitude regarding the initial velocity and range.

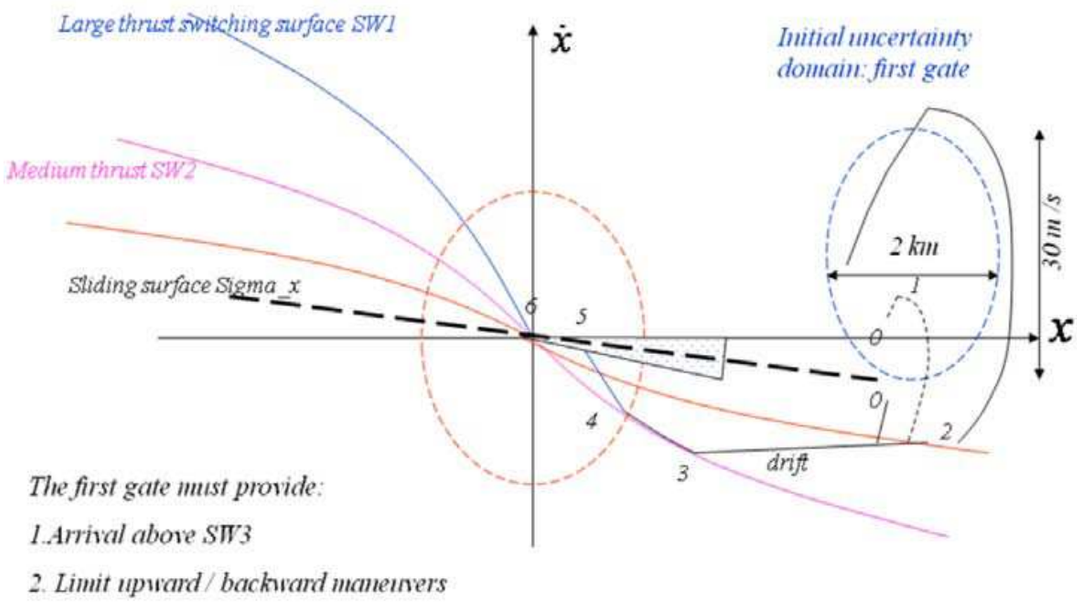

Fig. 13. First gate.

7. Use of active bitmap pixels to control relative attitude

Regulation of pursuer attitude for automated docking can be broken into two functional segments. While the objects are far apart, the pursuer's attitude is controlled to align its axial direction with the relative line of sight and to place its normal direction in the orbital plane. Control during this segment has been done many times and is not the subject of this discussion. When the objects are very close, and before docking can occur, the pursuer must align its mating surface with that of the pursued vessel. In this section, we discuss one practical method that this alignment can be performed efficiently, reliably and automatically.

Any geometry will do, but suppose that both mating surfaces are circular and that the target object is fitted with a series of detectable objects (i.e. lights) equally spaced around the mating surface. Suppose further that the pursuer is fitted with an array of suitable detectors which we shall call the Focal Plane Array (FPA) and that this FPA can be considered to lie in the center of its mating surface. As described in figure 14, if the surfaces are ready for docking, the pursuer will perceive a circular ring of lights in the center of the FPA. If the surfaces are offset, then the ring will be offset on the FPA. If the surfaces are misaligned, the ring will be elliptical rather than circular. The apparent size of this perceived ring of lights will indicate separation distance; the center will indicate normal and lateral error; the eccentricity of the ellipse will indicate the degree of angular error; and the orientation of the ellipse will indicate the relative axis about which the pursuer must rotate for successful docking. Although we will not address relative roll in this chapter, if one of the lights is

distinct from the others, a roll error could also be deduced. This is nearly equivalent to the information a human pilot would use to accomplish the same task.

Automated control of attitude for docking is thus reduced to two necessary tasks. First, information from the FPA must be interpreted (in the presence of noise) to yield a real-time measure of attitude error. Second, that error must be used to correctly orient the vehicle. We will apply a nonlinear least-squares curvefit and multidimensional search to the corrupted pattern of lights in order to estimate the equation of the perceived ellipse. The relative magnitude and orientation of the semi-major and semi-minor axes of this ellipse are used to generate a necessary angle of rotation and the unit vector we must rotate about, respectively. The relative degree approach will be used to generate a second-order sliding mode controller of the type described in (Levant, 2003). Finally, these methods will be implemented and tested using simulation.

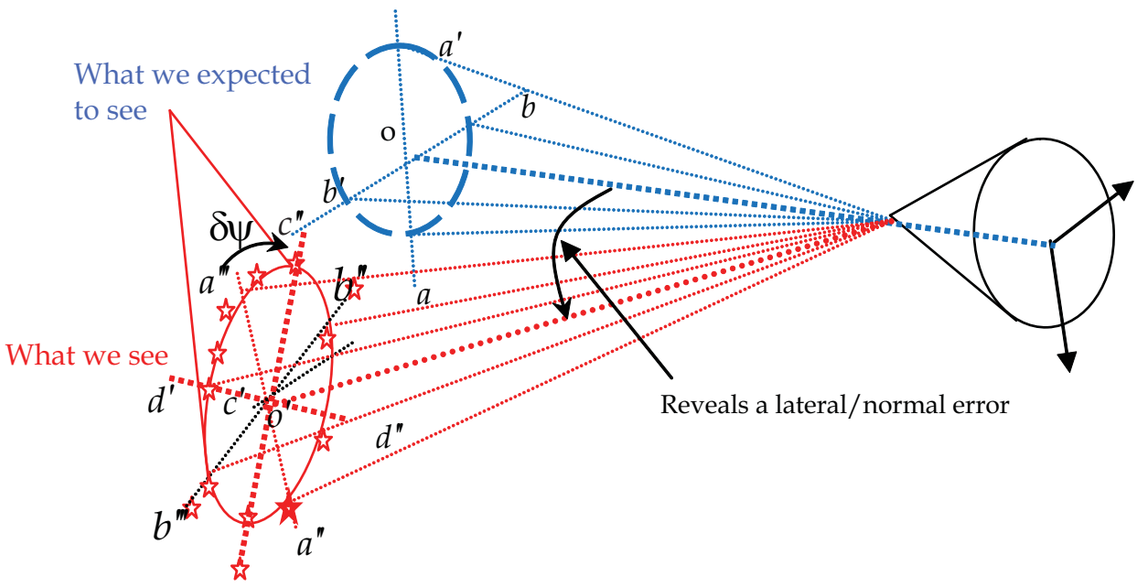

Fig. 14. Use of light patterns to extract relative position and attitude.

7.1 Mathematical background: Quaternions

The idea of relating two oriented surfaces (equivalently, two reference frames) by a single rotation about a specified axis is precisely the motivation behind the concept of quaternions. Since many readers will not be familiar with quaternions, we introduce a few important concepts here. Those wishing to understand quaternions in greater depth are referred to Dr. Kuipers' excellent book (Kuipers, 1999) on the subject.

Let us describe the relationship between two right-hand coordinate systems as a single rotation about a specified axis. Let us package this description into a 4-vector as follows:

$$\mathbf{Q} = \begin{bmatrix} \cos\eta \\ [\hat{\mathbf{u}}\sin\eta] \end{bmatrix} = \begin{bmatrix} \mathbf{q_0} \\ \mathbf{q} \end{bmatrix} \quad \begin{matrix} \eta = the\,magnitude\,of\,rotation \\ \hat{\mathbf{u}} = the\,(unit)\,vector\,to\,rotate\,about \end{matrix} \tag{22}$$

It is easily verified that this construct has (Euclidian) norm 1. If we define multiplication of these objects in a particular way, they exhibit several useful traits. Define:

$$\mathbf{PQ} = \mathbf{p}_0\mathbf{q}_0 - \mathbf{p}\bullet\mathbf{q} + \mathbf{p}_0\mathbf{q} + \mathbf{q}_0\mathbf{p} + \mathbf{p}\times\mathbf{q} \tag{23}$$

The following four useful and remarkable properties hold:

1. For any quaternion Q, $\mathbf{QQ}^* = \begin{bmatrix}\mathbf{q}_0\\ \mathbf{q}\end{bmatrix}\begin{bmatrix}\mathbf{q}_0\\ -\mathbf{q}\end{bmatrix} = \mathbf{Q}^*\mathbf{Q} = \begin{bmatrix}1 & 0 & 0 & 0\end{bmatrix}^t$ and this is the quaternion relating any coordinate frame to itself.
2. Given a vector v in the initial reference frame, the vector part of $\mathbf{Q}\begin{bmatrix}0\\ \mathbf{v}\end{bmatrix}\mathbf{Q}^*$ is the equivalent vector in the rotated frame.
3. Given quaternion P relating frame 1 to frame 2 and quaternion Q relating frame 2 to frame 3, the product QP is the quaternion relating 1 to frame 3.
4. If Q is the quaternion relating frame 1 to frame 2 and $\boldsymbol{\Omega} = \begin{bmatrix}\mathbf{pp}\\ \mathbf{qq}\\ \mathbf{rr}\end{bmatrix}$ represents the turning rate of frame 1 relative to frame 2 (i.e. the body rates) then $\dot{\mathbf{Q}} = \mathbf{Q}\begin{bmatrix}0\\ \boldsymbol{\Omega}\end{bmatrix}$

7.2 Attitude error from FPA measurements

In this exercise we are assuming that the pursuer's on-board sensor is the only source of attitude feedback. Specifically, this information takes the form of a set of Cartesian positions on the FPA corresponding to the location of the docking lights; with the detectors on the FPA working in the same way as rods on a human retina. Our challenge is to interpret, from this list of positions, the relative orientation of the pursuer and target docking surfaces.
As discussed in the introduction, if the docking surfaces are not perfectly adjusted, a circular pattern of indistinguishable lights (Fig. 15a) will appear as an offset ellipse (15b).

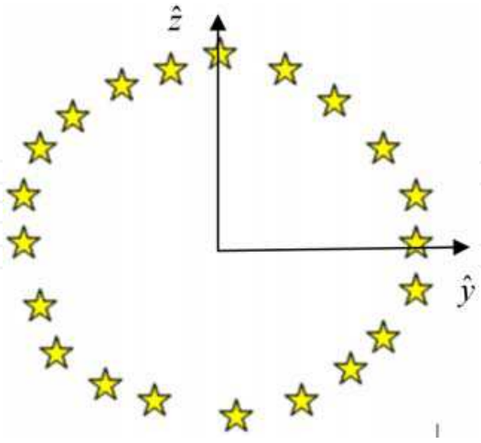

Fig. 15a. Circular pattern of docking lights.

Lateral and longitudinal guidance was described earlier in this chaper; thus we are only concerned that the pursuer's attitude be modified such that the percieved ellipse become circular. We proceed in two steps: first determine the equation of the ellipse that most nearly fits the measurements; then compute attitude error from this equation.

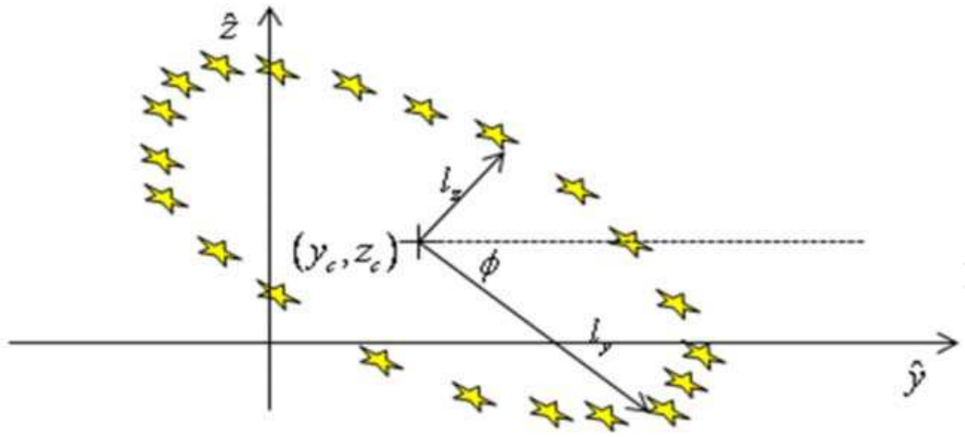

Fig. 15b. Docking lights as seen by pursuer.

The formal equation of an offset, rotated ellipse is:

$$\frac{\left((y-y_c)\cos\phi+(z-z_c)\sin\phi\right)^2}{l_y{}^2}+\frac{\left(-(y-y_c)\sin\phi+(z-z_c)\cos\phi\right)^2}{l_z{}^2}=1 \tag{24}$$

To perform least-squares curvefit from a set of measured points (x,z), define a function:

$$E=\sum_{all\,lights}\left\{1-\frac{\left((y-y_c)\cos\phi+(z-z_c)\sin\phi\right)^2}{l_y{}^2}+\frac{\left(-(y-y_c)\sin\phi+(z-z_c)\cos\phi\right)^2}{l_z{}^2}\right\}^2 \tag{25}$$

We will find a local minimum value of E with respect to the parameters $\{y_c, z_c, l_y, l_z, \phi\}$ using the steepest descent method:

$$\begin{bmatrix} y_c \\ z_c \\ l_y \\ l_z \\ \phi \end{bmatrix}_+ = \begin{bmatrix} y_c \\ z_c \\ l_y \\ l_z \\ \phi \end{bmatrix}_- - \frac{\rho}{\sqrt{\left(\partial E/\partial y_c\right)^2+\left(\partial E/\partial z_c\right)^2+\left(\partial E/\partial l_y\right)^2+\left(\partial E/\partial l_z\right)^2+\left(\partial E/\partial \phi\right)^2}} \begin{bmatrix} \partial E/\partial y_c \\ \partial E/\partial z_c \\ \partial E/\partial l_y \\ \partial E/\partial l_z \\ \partial E/\partial \phi \end{bmatrix} \tag{26}$$

with the ad-hoc addition that, if $E_+ > E_-$ then $\rho \leftarrow \frac{\rho}{10}$. This iteration is allowed to continue until the function E converges to a constant value at which the parameters describing the "best-fit" ellipse are established[3].

[3] The multivariate search described above requires an initial guess for each parameter. Convergence rate is sensitive to this guess and to the initial step size ρ. Furthermore, if care is not exercised, this search may converge to a local (and not global) minimum. An extensive discussion of multivariate search isoutside the scope of this chapter. outside the scope of this chapter.

The magnitude of rotation necessary for the ellipse to appear circular is described by:

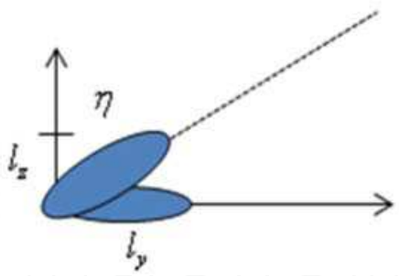

$$l_z = l_y \cos\eta \quad \Rightarrow \quad \eta = a\cos\frac{l_z}{l_y}$$

The required axis of rotation is the ellipse semi-major axis, which is described by:

$$\hat{\mathbf{u}} = \cos\phi\,\hat{\mathbf{y}} + \sin\phi\,\hat{\mathbf{z}} \tag{27}$$

The quaternion relating the pursuer's attitude to that necessary for docking is, therefore:

$$\mathbf{Q} = \begin{bmatrix} \cos\frac{\eta}{2} \\ 0 \\ \sin\frac{\eta}{2}\cos\phi \\ \sin\frac{\eta}{2}\sin\phi \end{bmatrix} = \begin{bmatrix} \sqrt{\frac{1}{2}\left(1 - l_z/l_y\right)} \\ 0 \\ \sqrt{\frac{1}{2}\left(1 + l_z/l_y\right)}\cos\phi \\ \sqrt{\frac{1}{2}\left(1 + l_z/l_y\right)}\sin\phi \end{bmatrix} \tag{28}$$

7.3 Derivation of the attitude control law

The relative degree approach to derivation of a control law consists of a sequence of general steps. First, establish an approximate mathematical model for the object to be controlled. If (as is always the case) this model is imperfect, we include an unknown "disturbance" function into which all of the uncertainties, approximations and unknowable quantities are swept. Second, the feedback error is defined. This error must be generated from measured quantities and must be positive definite. In the third step, a mathematical relationship is established between the feedback error and the actual control. This relationship is made to fit a template equation that is well-behaved in the presence of the expected disturbance. Finally, the relationship is solved to describe the necessary control in terms of the feedback error, possibly other measured quantities and the disturbance, which is discarded.

Let Q represent the quaternion relating the pursuer body frame to the required attitude for docking as computed in (24). In practice, the pursued vehicle may be rotating, but because we derive all our information from the pattern of docking lights, the pursued vehicle's rotation is confounded with the pursuing vehicle's rotation and is thus unknowable. Therefore we shall consider the desired attitude to be an inertial frame and consider any error resulting from this supposition to be part of the disturbance function. Further define:

$\mathbf{Q}_{\boldsymbol{\omega}} = \begin{bmatrix} pp \\ qq \\ rr \end{bmatrix}$ is the vector of the pursuer's body rates

$\mathbf{I} \in \mathbb{R}^{3x3}$ is the pursuer's matrix of inertia, which is considered nonsingular

$\begin{cases} \mathbf{B} \in \mathbb{R}^{3x3} \\ \mathbf{u} \in \mathbb{R}^{3} \end{cases}$ such that Bu represents the moment contribution of control in the body axis

The equations of state may be described as:

$$\begin{aligned} \dot{\mathbf{Q}} &= \mathbf{Q}\boldsymbol{\omega} + \boldsymbol{\Delta}_1 \\ \dot{\boldsymbol{\omega}} &= -\mathbf{I}^{-1}\boldsymbol{\omega} \times \mathbf{I}\boldsymbol{\omega} + \mathbf{I}^{-1}\mathbf{B}\mathbf{u} + \boldsymbol{\Delta}_2 \end{aligned} \tag{29}$$

For docking, we want the pursuer's body frame to align with the desired frame; this is equivalent to driving $\mathbf{Q} \to \begin{bmatrix} 1 & 0 & 0 & 0 \end{bmatrix}^t$. Because Q has norm 1, driving the vector part to zero will accomplish this desire. If we consider desired rotation about the body x-axis to be zero and restrict the remaining axis of rotation to quadrants 1 and 2 (accounting for the direction of rotation by other means) taking feedback error to be the vector part of Q results in a positive definite function. Therefore, with obvious notation, let:

$$\boldsymbol{\sigma} = [\mathbf{Q}]_{123} \tag{30}$$

ignoring disturbances and differentiating: $\dot{\boldsymbol{\sigma}} = [\mathbf{Q}\boldsymbol{\omega}]_{123}$

$$\ddot{\boldsymbol{\sigma}} = [\mathbf{Q}\mathbf{Q}\boldsymbol{\omega} + \mathbf{Q}\dot{\boldsymbol{\omega}}]_{123} = \left[\mathbf{Q}\mathbf{Q}\boldsymbol{\omega} + \mathbf{Q}(-\mathbf{I}^{-1}\boldsymbol{\omega} \times \mathbf{I}\boldsymbol{\omega} + \mathbf{I}^{-1}\mathbf{B}\mathbf{u})\right]_{123} \tag{31}$$

Before proceeding, we will need the following theorem:

Theorem: For quaternions $\mathbf{P} = \begin{bmatrix} \mathbf{p}_0 \\ [\mathbf{p}] \end{bmatrix}, \mathbf{Q} = \begin{bmatrix} \mathbf{q}_0 \\ [\mathbf{q}] \end{bmatrix}$, $\left\{\mathbf{P}^*[\mathbf{P}\mathbf{Q}]_{123}\right\}_{123} = \mathbf{p}_0\mathbf{q} + \mathbf{p}_0\mathbf{q}_0\mathbf{p}$ (32)

Proof: from Kuipers (p.108):

$$\mathbf{P}\mathbf{Q} = \begin{bmatrix} \mathbf{p}_0\mathbf{q}_0 - \mathbf{p}\bullet\mathbf{q} \\ [\mathbf{p}_0\mathbf{q} + \mathbf{q}_0\mathbf{p} + \mathbf{p} \times \mathbf{q}] \end{bmatrix}$$

$$\Rightarrow \quad \mathbf{P}^*[\mathbf{P}\mathbf{Q}]_{123} = \begin{bmatrix} \mathbf{p}_0(0) + \mathbf{p}\bullet(\mathbf{p}_0\mathbf{q} + \mathbf{q}_0\mathbf{p} + \mathbf{p} \times \mathbf{q}) \\ \left[\mathbf{p}_0(\mathbf{p}_0\mathbf{q} + \mathbf{q}_0\mathbf{p} + \mathbf{p} \times \mathbf{q}) - (0)\mathbf{p} - \mathbf{p} \times (\mathbf{p}_0\mathbf{q} + \mathbf{q}_0\mathbf{p} + \mathbf{p} \times \mathbf{q})\right] \end{bmatrix}$$

$$\begin{aligned} \left\{\mathbf{P}^*[\mathbf{P}\mathbf{Q}]_{123}\right\}_{123} &= \mathbf{p}_0{}^2\mathbf{q} + \mathbf{p}_0\mathbf{q}_0\mathbf{p} + \mathbf{p}_0(\mathbf{p} \times \mathbf{q}) - \mathbf{p}_0(\mathbf{p} \times \mathbf{q}) - \mathbf{q}_0(\mathbf{p} \times \mathbf{p}) - \mathbf{p} \times \mathbf{p} \times \mathbf{q} \\ &= \mathbf{p}_0{}^2 q + \mathbf{p}_0\mathbf{q}_0\mathbf{p} \end{aligned}$$

□

Define:

$$\mathbf{S}(\dot{\boldsymbol{\sigma}}, \boldsymbol{\sigma})_{1,2,3} = -\rho\,\mathbf{SIGN}\left(\dot{\sigma}_{1,2,3} + \mu\left|\sigma_{1,2,3}\right|^{1/2} sign(\sigma_{1,2,3})\right) \text{ where } \rho \text{ and } \mu \text{ are positive constants.} \tag{33}$$

It is shown [26] that the equation: $\ddot{\boldsymbol{\sigma}}_{1,2,3} - \mathbf{S}(\dot{\boldsymbol{\sigma}}, \boldsymbol{\sigma})_{1,2,3} = \boldsymbol{\Delta}_{1,2,3}$ is finite-time stable and displays "good" transient behavior in each of its three elements so long as elements of the disturbance Δ are bounded by the proportionality constant ρ. Substituting for the second derivative in (31):

$$\mathbf{S} = \left[\mathbf{QQ\omega} + \mathbf{Q}(-\mathbf{I}^{-1}\boldsymbol{\omega} \times \mathbf{I\omega} + \mathbf{I}^{-1}\mathbf{Bu}) \right]_{123}$$

Pre-multiply both sides by $\mathbf{Q}^*$ and apply the theorem:

$$\mathbf{Q}^*\mathbf{S} = \mathbf{Q}^* \left[\mathbf{QQ\omega} \right]_{123} + \mathbf{Q}^* \left[\mathbf{Q}\left(-\mathbf{I}^{-1}\boldsymbol{\omega} \times \mathbf{I\omega} + \mathbf{I}^{-1}\mathbf{Bu} \right) \right]_{123}$$

$$\left[\mathbf{Q}^*\mathbf{S} \right]_{123} = \mathbf{q}_0{}^2 \left[\mathbf{Q\omega} \right]_{123} + \mathbf{q}_0 \left[\mathbf{Q\omega} \right]_0 \left[\mathbf{Q}^* \right]_{123} - \mathbf{q}_0{}^2 (\mathbf{I}^{-1}\boldsymbol{\omega} \times \mathbf{I\omega}) + \mathbf{q}_0{}^2 (\mathbf{I}^{-1}\mathbf{Bu})$$

Solve for the control u:

$$\mathbf{u} = \mathbf{B}^{-1}\mathbf{I} \left\{ \frac{1}{\mathbf{q}_0{}^2} \left[\mathbf{Q}^*\mathbf{S} \right]_{123} - \left[\mathbf{Q\omega} \right]_{123} + \frac{\left[\mathbf{Q\omega} \right]_0}{q_0} \left[\mathbf{Q} \right]_{123} - (\mathbf{I}^{-1}\boldsymbol{\omega} \times \mathbf{I\omega}) \right\} \tag{34}$$

7.4 Simulation results

In order to demonstrate this method of attitude control for automated docking, a ten-second interval near the end of a docking mission was simulated. The initial separation is 11 m and the closing velocity is 1 m/sec. Lateral and longitudinal control are not included in this exercise, nor is roll attitude. Initially, the docking surfaces are misaligned by .1 radian (~6 degrees) in the pitch direction and .25 radians(14 degrees) in yaw. Additionally, we have initial body rates equal to .05 rad/sec away from zero in the pitch and .1 rad/sec towards zero in yaw. Realistically, seeker error would decrease as the surfaces approach, but for demonstration purposes, a uniformly-distributed 5% error was added to the y- and z-positions of each docking light.

The gains ρ and μ of Eq. (33) were empirically set to 5 and 0.25, respectively; these gains were intentionally not fine-tuned and it was observed that acceptable behavior is exhibited when either or both of these are halved or doubled.

Results are summarized in Figs. 16 – 18.

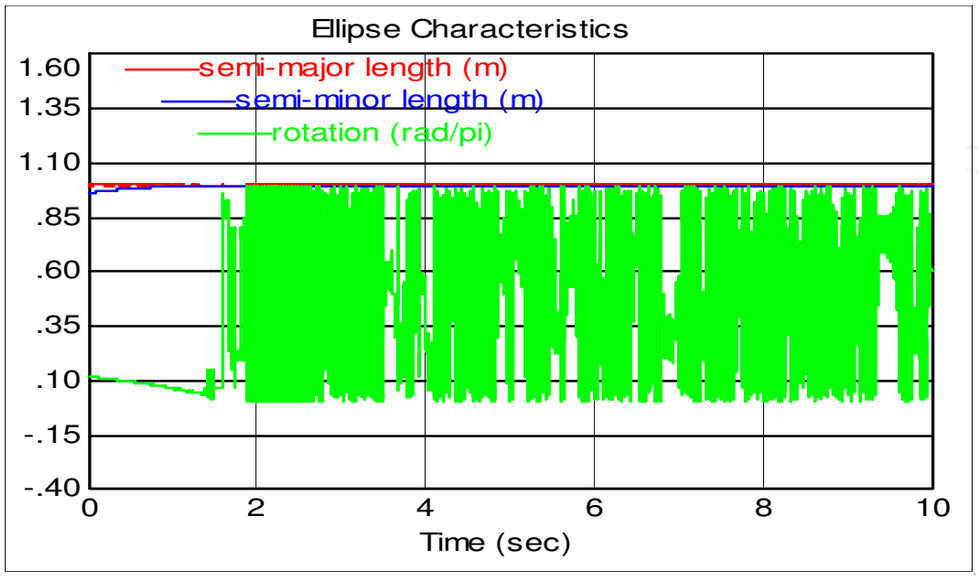

Fig. 16. Characteristics of the curvefit ellipse.

In Fig. 16 we observe that the (normalized) semi-major axis length is constant at unity. This is necessary, as the apparent length (adjusting for changes in proximity) does not change with aspect. The semi-minor axis length is initially somewhat less, but quickly converges to one; this is an indication that the percieved ellipse becomes a percieved circle. At about the time the semi-minor axis approaches unity, the apparent rotation of the ellipse becomes chaotic. This is expected – as the FPA image becomes more circular, definition of the semi-major and semi-minor axes is largely determined by noise.

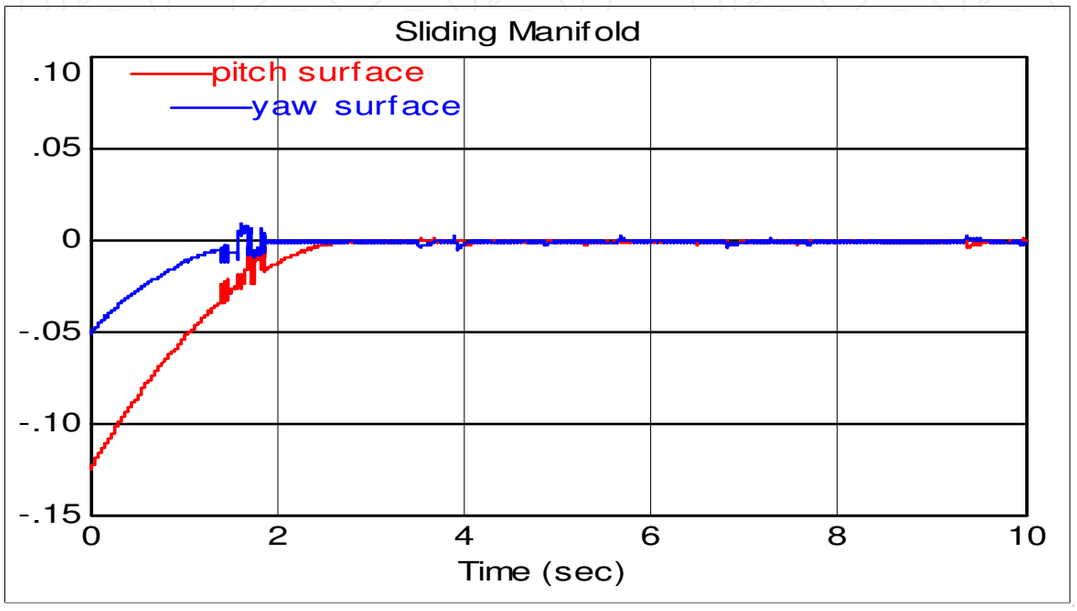

Fig. 17. Quaternion elements 2 and 3.

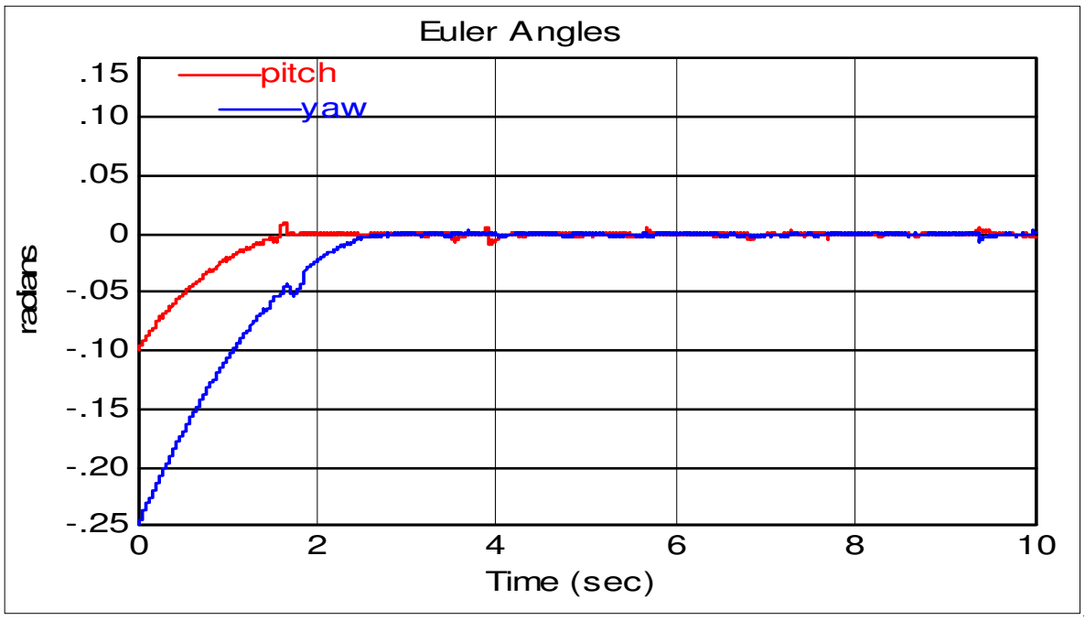

Fig. 18. Corresponding pitch and yaw angles.

In Fig. 17 we observe that the sliding variables are driven into a narrow band about zero in finite time and remain within that band thereafter. Note that actual convergence to the sliding surface occurs significantly after the quaternion axis (green line of Fig. 16) becomes chaotic. It is apparent that the averaged reaction to extremely noisy feedback is still useful for control. If the seeker noise was correlated in time, we might expect to see a small and persistent error away from zero.

Euler angles are easily extracted from the quaternion elements. In Fig. 18 we see the pitch misalignment, which started nearer to zero converge first, followed by yaw. After the transient, both angles are constrained to within about 3 or 4 milliradians (0.2 degrees). Speed of convergence and ultimate boundary are largely dictated by the gains ρ and μ of Eq. (33), subject to limitations on thruster force and the need to dominate the sum of all disturbances.

7.5 Observations

Before concluding this section, let us make some interesting and important observations concerning the demonstrated method for automatic control of attitude for docking.

First, this automated method is very similar to the approach taken by a human pilot; rather than assembling position and attitude information from a variety of sources, computing a time profile and inverting the physical model to produce attitude commands, this method "sees" that the ring of docking lights is slightly out of round and nudges the controls in response. This not only increases confidence in the robustness of our method, but introduces the possibility of Human Assisted Control (HAC) for docking attitude.

Second, there is no Inertial Measuring Device (IMU) input involved in this method. This means no IMU errors, no acquisition and processing of IMU data, no synchronization of IMUs between the pursuer and pursued and no provisioning for loss of data. All feedback is from a single, reliable on-board source. On a related note, there is no participation required on the part of the pursued object and no communication requirement. This is extremely favorable because communication increases risk and always introduces delay. Delay is extremely detrimental to sliding mode control, which is fundamentally based on high-frequency switching.

Finally, the reader may have spotted a significant flaw in our method. When interpreting the ring of docking lights as an ellipse on the FPA, the magnitude of rotation and the axis of rotation can be determined, but there is no inherent way to determine the direction of rotation. In other words, we cannot tell if the ellipse is tipped "towards" us or "away". This perceptive reader is correct; some other method such as Doppler ranging or a comparison of the relative brightness on each side of the semi-major axis must be used to supply this final bit of information. While generating the results of Figs. 16-18, we assumed that the directionality was known and correct.

7.6 Conclusion: Attitude control

It is possible to control relative attitude by simply constructing a quaternion error function of the pattern of lights. One must note that the algorithm process is very similar to the human control processes in that the idea is to drive errors to zero. These solutions are enabled by the property that sliding mode controllers are perfectly insensitive to matched disturbances. Using this property it is possible to not represent explicitly in the design some dynamical terms of the sliding variable dynamics and to treat them simply as disturbance terms.

8. Chapter conclusion

The simplicity and elegance of the solution is a unique attribute of this emerging technique which makes it a *game changer.* Proposed design could conciliate the optimality of bang-bang solutions which are not robust with the robustness of HOSM which is not optimum. The result is a very simple design that conciliates a quasi-optimality with a perfect robustness. The insensitivity property of HOSM controllers to matched disturbances allowed to treat all the dynamical effects other than caused by the control to be treated as disturbances and compensated implicitly. Likewise for the attitude motion where by treating all dynamical effects other than the torques created by attitude command thrusters the three attitude motions could be treated as explicitly de-coupled[4] which greatly simplified the design of the control. Finally by running the simulation for a very long duration we showed that final results of extreme accuracy could be achieved.

9. References

W. A. Chobotov. (2002). *Orbital Mechanics (3rd Ed.)*. AIAA Educational Series, Reston VA. pp. 155-158.

C. Edwards. And S. Spurgeon S. (1998). *Sliding Mode Control: Theory and Applications*.

Taylor & Francis, Bristol. ESA (2006) Document No. EUC-ESA-FSH-003 REV-1.2.

L. Fridman, Y. Shtessel, C. Edwards, and X. G. Yan. (2008). Higher Order Sliding Mode Observer for State Estimation and Input Reconstruction in Nonlinear Systems. *International Journal of Robust and Nonlinear Control, Special Issue on Advances in Higher Order Sliding Mode Control,* Vol. 18, Issue 4-5 (March). pp. 399-412.

C. Hall and Y. Shtessel. (2006). Sliding Mode Disturbance Observers-based Control for a Reusable Launch Vehicle. *AIAA Journal on Guidance, Control, and Dynamics*, Vol. 29, No. 6, (November-December). pp. 1315-1329.

C. D. Karlgard. (2006). Spacecraft. *AIAA Journal of Guidance, Control, and Dynamics,* Vol. 29, No. 1. pp. 495-499.

J. Kuipers. (1999). *Quaternions and Rotation Sequences*. Princeton University Press, Princeton NJ

A. Levant. (2001). Universal SISO sliding-mode controllers with finite-time convergence. IEEE Transactions on Automatic Control, Vol. 46, No. 9. pp. 1447-1451.

A. Levant. (2003). Higher-order sliding modes, differentiation and output-feedback control. *International Journal of Control*. Vol. 76, No. 9/10. pp. 924-941.

T. Massey and Y. Shtessel. (2005). Continuous Traditional and High Order Sliding Modes for Satellite Formation Control. *AIAA Journal on Guidance, Control, and Dynamics,* Vol. 28, No. 4, (July-August). pp. 826-831.

I. A. Shkolnikov, Y. B. Shtessel, M. Whorton, and M. Jackson. (2000). Robust to Noise Microgravity Isolation Control System Design via High-Order Sliding Mode Control. *Proceedings of the Conference on Guidance, Navigation, and Control,* Denver, CO. AIAA paper No. 2000-3954.

[4] The coupling between attitude channels is treated as disturbance and is thus, compensated implicitly by the controller

I. Shkolnikov, Y.B. Shtessel, and D. Lianos. (2005). The effect of sliding mode observers in the homing guidance loop,. *ImechE Journal on Aerospace Engineering,* Part G, 219, 2. pp. 103-111.

Y. Shtessel, C. Hall, and M. Jackson. (2000). Reusable Launch Vehicle Control in Multiple Time Scale Sliding Modes. *AIAA Journal on Guidance, Control, and Dynamics,* Vol. 23, No. 6. pp. 1013-1020

Y.B. Shtessel, I. Shkolnikov, and M. Brown. (2003). An Asymptotic Second-Order Smooth Sliding Mode Control. *Asian Journal of Control*, Vol. 4, No. 5. pp. 498-504.

Y. Shtessel, I. Shkolnikov and A. Levant. (2007). Smooth Second Order Sliding Modes: Missile Guidance Application. *Automatica*, Vol. 43, No.8. pp. 1470-1476.

Y. Shtessel, S. Baev, C. Edwards, and S. Spurgeon. (2010). HOSM observer for a class of non-minimum phase causal nonlinear MIMO systems. *IEEE Transactions on Automatic Control*, Vol. 55, No. 2. pp. 543-548.

P. Singla, K. Subbarao, and J. L. Junking. (2006) Adaptive Output Feedback Control for Spacecraft Rendezvous and Docking under Measurement Uncertainty. *AIAA Journal of Guidance, Control, and Dynamics,* Vol. 22, No. 4. pp. 892-902.

A. Sparks. (2000). Satellite Formation Keeping in the Presence of Gravity Perturbations, *Proceedings of the American Control Conference (*June).

C. Tournes, and Y.B. Shtessel. (2006). Autopilot for Missiles Steered by Aerodynamic Lift and Divert Thrusters using Second-Order Sliding Mode. *AIAA Journal of Guidance Control and Dynamics* Vol. 29, No. 3. pp. 617-623.

C. Tournes, Y.B. Shtessel. (2007). Automatic Docking using Second Order Sliding Mode Control. *Proceedings of the 2007 IEEE American Control Conference.*

V. Utkin, J. Guldner, and J. Shi. (1999). *Sliding Modes in Electromechanical Systems*. Taylor and Francis, London.

P. K. Wang, F. Y. Hadaegh and K. Lau. (1999) Synchronized Formation Rotation and Attitude Control of Multiple Free-Flying Spacecrafts. *AIAA Journal of Guidance, Control, and Dynamics,* Vol. 29, No. 1. pp. 28-35.

H. Wong, V, Karpila. (2001). Adaptive Output Feedback Tracking Control of Multiple Spacecraft. *Proceedings of the American Control Conference, (*June).

Sliding Mode Control

Edited by Prof. Andrzej Bartoszewicz

ISBN 978-953-307-162-6
Hard cover, 544 pages
Publisher InTech
Published online 11, April, 2011
Published in print edition April, 2011

The main objective of this monograph is to present a broad range of well worked out, recent application studies as well as theoretical contributions in the field of sliding mode control system analysis and design. The contributions presented here include new theoretical developments as well as successful applications of variable structure controllers primarily in the field of power electronics, electric drives and motion steering systems. They enrich the current state of the art, and motivate and encourage new ideas and solutions in the sliding mode control area.

InTech Europe
University Campus STeP Ri
Slavka Krautzeka 83/A
51000 Rijeka, Croatia
Phone: +385 (51) 770 447
Fax: +385 (51) 686 166
www.intechopen.com

InTech China
Unit 405, Office Block, Hotel Equatorial Shanghai
No.65, Yan An Road (West), Shanghai, 200040, China
中国上海市延安西路65号上海国际贵都大饭店办公楼405单元
Phone: +86-21-62489820
Fax: +86-21-62489821

IntechOpen